ELSEVIER

A theoretical study of the original Shilov reaction involving methane activation by platinum tetrachloride ($PtCl_4^{2-}$) in an acidic aqueous solution

Hongjuan Zhu, Tom Ziegler *

Department of Chemistry, University of Calgary, 2500 University Drive, N.W. Calgary, Alberta, Canada T2N 1N4

Abstract

Density functional theory (DFT) has been employed to investigate the rate-determining step for the Shilov reaction in which $PtCl_4^{2-}$ can catalyze H–D exchange of alkanes in acidic aqueous solution. C–H activation and methane uptake are the two possible candidates. Associative and dissociative pathways are both considered in the methane uptake step. It was not possible to determine whether methane uptake followed an associative or dissociative mechanism due to uncertainties in the calculated contributions to the free energy of activation from entropy and solvation. The active species in the Shilov reaction are $PtCl_4^{2-}$, $PtCl_3H_2O^-$ and $PtCl_2(H_2O)_2$. We have shown that $PtCl_2(H_2O)_2$ is the most active catalyst for H/D exchange. Rate expressions for the Shilov reaction have been derived for different reaction conditions.
© 2006 Elsevier B.V. All rights reserved.

Keywords: Shilov reaction; C–H activation; Density functional theory

1. Introduction

The activation of C–H bonds in alkanes has considerable industrial potential as the first step in the conversion of abundant hydrocarbons to more valuable chemicals. One of the first homogeneous catalysts for C–H activation was discovered by Shilov et al. in 1969 when they found that platinum tetrachloride ($PtCl_4^{2-}$) could catalyze H–D exchange of alkanes in acidic aqueous solution [1]. This reaction was shortly after investigated in detail by Hodges et al. [2]. A mechanism for H–D exchange has been suggested in which an alkane first binds to platinum followed by C–H cleavage, solvent mediated H^+/D^+ exchange and finally elimination of the deuterated alkane (Scheme 1).
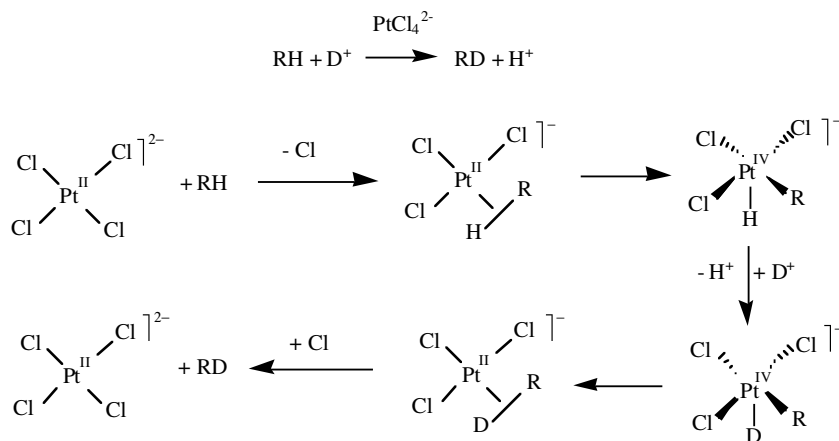
In 1972, Shilov et al. found that $PtCl_4^{2-}$ can catalyze the functionalization of alkanes with $H_2[PtCl_6]$ as the oxidant [3]. A mechanism for the observed alkane functionalization has been put forward by Shilov and others (Scheme 2). In this scheme, the platinum (II) complex **A** activates the alkane and generates an alkylplatinum (II) intermediate **B**. The alkylplatinum (II) intermediate **B** is subsequently oxidized by platinum (IV) to the alkylplatinum (IV) species **C**. Finally, the alkylplatinum (IV) species **C** reductively eliminates RX to afford the oxidized alkane with regeneration of the Pt (II) catalyst **A**. Because of the use of the expensive oxidant Pt(IV), this reaction has not been implemented on an industrial scale.
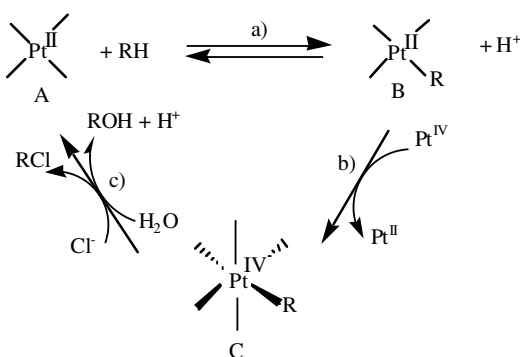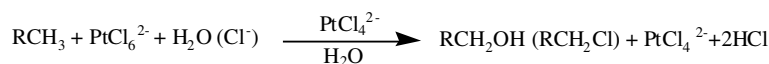
A number of theoretical and experimental studies have been carried out in order to identify the rate-determining step in the Shilov process of Schemes 1 and 2, with the focus on alkane uptake or C–H activation as possible candidates. Siegbahn and Crabtree [4] have conducted a theoretical study on methane activation by $PtCl_2(H_2O)_2$ where they found that C–H activation was the rate-determining step. On the other hand, Hush et al. [5] studied methane activation by the somewhat different catalyst $PtCl_2(NH_3)_2$ and

---

* Corresponding author.
  E-mail address: ziegler@ucalgary.ca (T. Ziegler).

$$RH + D^+ \xrightarrow{\text{PtCl}_4{}^{2-}} RD + H^+$$

Scheme 1. Mechanism for H–D exchange in the Shilov reaction.

$$RCH_3 + PtCl_6{}^{2-} + H_2O\,(Cl^-) \xrightarrow[\text{H}_2\text{O}]{\text{PtCl}_4{}^{2-}} RCH_2OH\,(RCH_2Cl) + PtCl_4{}^{2-} + 2HCl$$

Scheme 2. Proposed catalytic cycle for the platinum-catalyzed oxidation of alkanes in aqueous solution.

calculated that uptake of methane was rate determining. Experimentally, Bercaw et al. [6] found for a related system $[(N–N)Pt(CH_3)(solv)]^+ BF_4^-$ with N–N = ArN=C(Me)C-(Me)=NAr and Ar = 2,6(CH_3)_2C_6H_3, where solv = CF_3-CH_2OH that uptake of methane is rate determining with a free energy barrier of 23.10 kcal/mol. It is thus likely that the relative rate of CH_4 uptake and C–H activation is strongly depend on the nature of the auxiliary ligands.

Gol'dshleger and Shteinman [7] studied the influence of the auxiliary ligands on the rate of the Shilov reaction. They used a series of different platinum complexes $PtCl_2S_2$ (S = H_2O, Cl^-, Br^-, I^-, NO_2^-, PPh_3, CN^-) and found that the rate of the deuterium exchange decreases in the order of $H_2O > Cl^- > Br^- > I^- > NO_2^- > PPh_3 > CN^-$. Thus, this study demonstrated that the H–D exchange rate is inversely proportional to the *trans*-directing power of the ligand S. In addition, Shteinman et al. determined the kinetic parameters in the H–D exchange of cyclohexane as $\Delta S^{\neq} = -22.6$ e.u. and $\Delta H^{\neq} = 17.5$ kcal/mol for the overall rate when S is H_2O.

The objective of the current investigation has been to assess C–H activation and methane uptake as possible can-

didates for the rate determining step in the Shilov reaction. For the methane uptake, both a dissociative and associative mechanisms will be considered. Ultimately, our findings will be used to identify the rate determining step for the H^+/D^+ exchange catalyzed by $PtCl_4^{2-}$ and $PtCl_2(H_2O)_2$, respectively [1,7], as well as the most active species involved in this transformation.

2. Computational details

Results were obtained from DFT calculations based on the Becke–Perdew exchange-correlation functional [8–10], using the Amsterdam density functional (ADF) program [11]. The standard double-ζ STO bases with one set of polarization functions were applied for H, N, and O atoms, while the standard triple-ζ basis sets were employed for Cl and Pt atoms. The 1s electrons of N and O, as well as the 1s–2p electrons of Cl and 1s–4f electrons of Pt, were treated as frozen core. The standard set of auxiliary s, p, d, f and g STO functions, centered on each nucleus, was used to fit the electron density and calculate the Coulomb and exchange potentials in each SCF cycle. Reported energies

include first-order scalar relativistic corrections [12]. Gas-phase electronic enthalpies were calculated from the Kohn–Sham energies. In all free energy values reported, the electronic entropy was neglected and standard expressions [13] were used to calculate the remaining gas-phase enthalpic and entropic contributions at nonzero temperature, including the zero-point vibrational contribution.

Thermodynamic parameters for the solvation of the chloride ion were obtained from a recent compilation of experimental values [14]. The remaining solvation enthalpies (included for both single-point calculations and geometry optimizations) were obtained using the COSMO [15] method as implemented in ADF [16]. The solvent excluding surface was used along with an epsilon value of 78.4 for the dielectric constant of water as the solvent. Atomic radii employed were 1.39, 1.8, 1.16, 1.4 and 1.3 Å for Pt, Cl, H, N, and O, respectively. Although the Born energy reported by the COSMO model is, strictly speaking, a free energy, the entropic contribution accounts to perhaps 2% of the total energy [17]. The solvation enthalpy was therefore taken as the difference between the gas-phase energy and that calculated using the COSMO solvation model.

For the purpose of calculating the remaining solvation entropies, the solvation process was broken up into three steps, following Wertz [18]. Here, the solute in the gas phase is first compressed to the molar volume of the solvent. The compressed solute gas then loses the same fraction of its entropy as would be lost by the solvent in going from gas (at its liquid-phase density) to liquid. Finally, the solute gas is extended to the density of the desired solution (i.e., 1.0 L/mol).

The solute entropy change for the first and third steps, which are strictly changes in molar volume, is given by $\Delta S = R \ln(V_{m,f}/V_{m,I})$, where $V_{m,f}$ is the final solute molar volume and $V_{m,I}$ is the initial solute value. The entropy fraction α lost in the second step can be determined from the absolute entropies of the solvent in its gas (S_{gas}°) and liquid (S_{liq}°) phases, as shown in the following equation:

$$\alpha = \frac{S_{liq}^{\circ} - \left(S_{gas}^{\circ} + R \ln V_{m,liq}/V_{m,gas}\right)}{\left(S_{gas}^{\circ} + R \ln V_{m,liq}/V_{m,gas}\right)}. \qquad (1)$$

Substituting the appropriate parameters for water [19], we have $\alpha = -0.46$. The sum of the entropy changes accompanying each of the three steps then gives the total solvation entropy; at a temperature of 298.15 K, we have (again, for water) the following equation:

$$\Delta S_{sol} = (-14.3 \text{ cal mol}^{-1} \text{ K}^{-1})$$
$$- 0.46(S^{\circ} - 14.3 \text{ cal mol}^{-1} \text{ K}^{-1})$$
$$+ (7.98 \text{ cal mol}^{-1} \text{ K}^{-1}). \qquad (2)$$

It is convenient that (by chance) the constant in Eq. (2) very nearly cancel on expansion, and the solvation entropy in water can therefore be approximated in more qualitative discussions as 50% of the gas-phase entropy, with the opposite sign.

3. Results and discussion

We shall begin our exposition by a discussion of the species that might be involved in the H/D exchange reaction of Scheme 1.

3.1. Distribution of different platinum species in aqueous solution

When platinum tetrachloride ($PtCl_4^{2-}$) dissolves in aqueous solution, its chloride ligands can be substituted by water molecules one by one leading to mono-, di-, tri- and tetra-aquo platinum complexes. The concentration ratios of the different aquo platinum species depend on the concentration of chloride ions (Cl^-) added to the solution in excess of those originating from $PtCl_4^{2-}$.

Table 1 displays the calculated equilibrium constants involving species originating from aquation of $PtCl_4^{2-}$. Free energies of all species involved in the aquation of $PtCl_4^{2-}$ have been calculated in order to determine the equilibrium constants. It follows from Table 1 that our calculated equilibrium constants compare well with those obtained experimentally. The good agreement provides some justification for the solvation model used in the current investigation. Fig. 1 displays the ratio of the different aqua platinum complexes as a function of the free chloride concentration.

In the Shilov reaction, 0.2 M of chloride ions is added to a 0.02 M K_2PtCl_4 solution. It thus follows from the calculated equilibrium constants of Table 1 that tetrachloroplatinum ($PtCl_4^{2-}$) is the dominant species (∼95.8%), followed by monoaqua-trichloroplatinum ($PtCl_3H_2O^-$) (∼4.17%) and diaqua-dichloroplatinum ($PtCl_2(H_2O)_2$) (∼0.005%), the other two species, $PtCl(H_2O)_3^+$ and $Pt(H_2O)_4^{2+}$, have negligible concentrations. In the Shteinman reaction, 0.0043 M of $PtCl_2(H_2O)_2$ in aqueous solution is used with no external Cl^- added. Thus, $PtCl_2(H_2O)_2$ is the main species (∼85.61%), followed by $PtCl(H_2O)_3^+$ (∼7.175%), $PtCl_3H_2O^-$ (∼7.145%), $Pt(H_2O)_4^{2+}$ (∼0.053%) and $PtCl_4^{2-}$ (∼0.017%).

In the Shilov and Shteinman reactions, an alkane hydrogen is exchanged by a deuterium atom from a solvent molecule. We shall in the following study alkane uptake by a Pt-complex and C–H activation by the platinum center as

Table 1
Equilibrium constants for aqualization reactions of platinum tetrachloride ($PtCl_4^{2-}$) in water

Reactions	ΔG (kcal/mol)	Equilibrium constant[b]
$PtCl_4^{2-} + H_2O \rightarrow PtCl_3H_2O^- + Cl^-$	2.81	0.87×10^{-2} (3.0×10^{-2})[a]
$PtCl_3(H_2O)^- + H_2O \rightarrow PtCl_2(H_2O)_2 + Cl^-$	4.91	0.25×10^{-3} (1.0×10^{-3})[a]
$PtCl_2(H_2O)_2 + H_2O \rightarrow PtCl(H_2O)_3^+ + Cl^-$	7.85	1.76×10^{-6}
$PPtCl(H_2O)_3^+ + H_2O \rightarrow Pt(H_2O)_4^{2+} + Cl^-$	9.29	1.55×10^{-7}

[a] Experimental values from Refs. [20–23] are shown in the parenthesis.
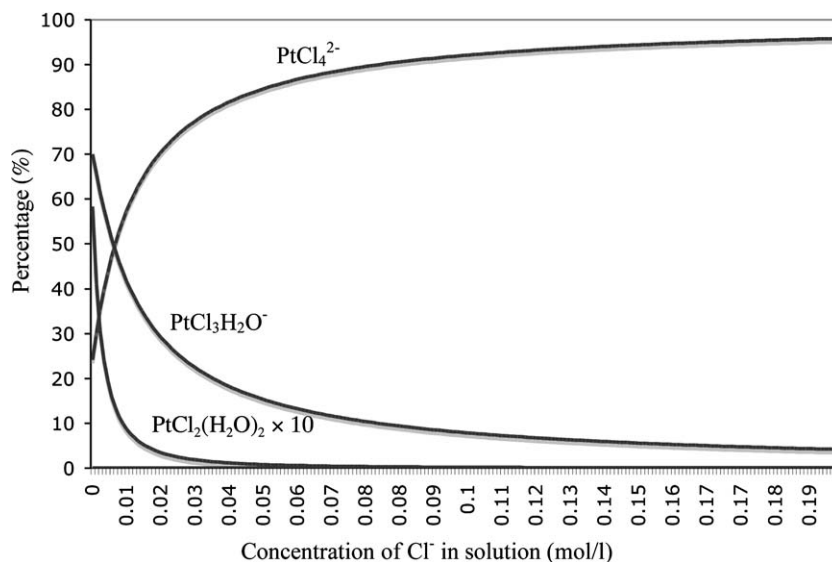[b] Calculated at 298 K.

Fig. 1. Ratio of different platinum species in $PtCl_4^{2-}$ aqueous solution as a function of the concentration of Cl^- in solution.

possible rate determining steps in the H/D exchange, see Scheme 1. The alkane will be modeled by methane.

3.2. Possible mechanisms for the uptake of methane

The first step in the H/D exchange reaction of Scheme 1 is the uptake of methane. Methane uptake can take place in a dissociative or associative fashion. In the dissociative mechanism, the platinum complex loses first one ligand, after that, methane binds to platinum taking over the coordination site of the leaving ligand (Scheme 3). In the associative mechanism, the leaving ligand is departing and the entering ligand is approaching the platinum at the same

time. A distorted trigonal-bipyramidal transition state is formed followed by elimination of the leaving ligand and formation of the product (Scheme 4).

Bercaw et al. have found from activation volume measurements [24] that the substitution of a solvent molecule by benzene at the platinum (II) methyl cation [(N–N)Pt-$(CH_3)(solv)]^+$ (N–N = ArN=C(Me)C(Me)=NAr, Ar = 2, 6-$(CH_3)_2C_6H_3$, solv = CF_3CH_2OH) takes place via an associative mechanism. The substitution of ligands in square planar Pt(II) complexes is in general assumed to take place by an associative mechanism [25–27]. We shall now turn to a discussion of the associative and dissociative uptake of methane.
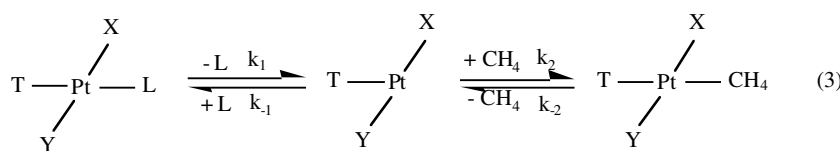
$$k_D = \frac{[PtXYTL]\, k_1 k_2\, [CH_4]}{k_{-1}\,[L] + k_2\,[CH_4]} \qquad (4)$$

Scheme 3. Mechanism and overall rate for the dissociative uptake of methane by a square-planar platinum complex.
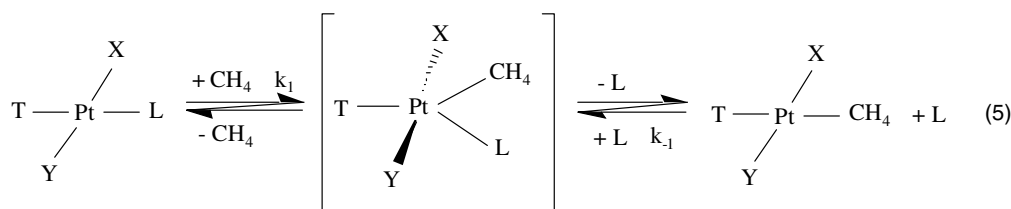
$$k_A = k_1\,[PtXYTL][CH_4] \qquad (6)$$

Scheme 4. Mechanism and overall rate of the associative uptake of methane by a square-planar platinum complex.

3.3. Associative mechanism for methane uptake

The uptake of methane by $PtCl_4^{2-}$, $PtCl_3H_2O^-$ and $PtCl_2(H_2O)_2$ give rise to eight possible reactions as shown in Scheme 5. We present the calculated thermodynamic and kinetic data for the eight associative methane uptake reactions in Table 2. The associative transition state structures for the methane uptake reactions I–VIII are displayed in Fig. 2.

All the uptake reactions are endothermic as the Pt–Cl and Pt–H_2O bonds broken are stronger than the Pt–CH_4 bond formed. The substitution reactions in which methane replaces Cl^- have a positive reaction entropy due to the net loss of rotational entropy as CH_4 is coordinated. The reaction entropy is much smaller for the substitution of H_2O where the loss of rotational entropy for CH_4 is compensated for in part by the gain of rotational entropy for H_2O.

It can be seen from Table 3 that the bond dissociation enthalphies follow the order ΔH (Pt–H_2O) trans to $Cl^- < \Delta H$ (Pt–Cl) trans to $Cl^- \sim \Delta H$ (Pt–H_2O) trans to $H_2O < \Delta H$ (Pt–Cl) trans to H_2O. This is consistent with that Cl^- binds more strongly to platinum than H_2O and that Cl^- is more trans-stabilizing. The optimized structures of $PtCl_4^{2-}$, $PtCl_3(H_2O)^-$ and $PtCl_2(H_2O)_2$ are given in Fig. 3.

The general trends in the bond enthalpies discussed above result in the following order for the methane uptake

reaction enthalpies: (II, V) < (I, VII, III, VI) < (IV, VIII). See Table 2. All the reactions are endothermic, the corresponding transition states are all late with considerable bond breaking between platinum and the leaving group and only a weakly emerging bonding between platinum and methane. See Fig. 2. The two reactions with the lowest barriers, II and V, are the two least endothermic processes corresponding to the substitution of H_2O trans to chlorine. The transition states are as expected "earlier" than for the other reactions with II of lowest barrier having the longest Pt–CH_4 distance of 3.07 Å followed by V with Pt–CH_4 = 2.94 Å.

The two processes (IV, VIII) with the highest barriers are also the reactions with the highest endothermicities. They correspond to the substitution of Cl^- trans to water and have transition state structures with Pt–CH_4 distances of 2.65 Å (IV) and 2.64 Å (VIII), respectively, see Fig. 2.

Finally, the four substitution reactions (VII, III, I, VI) with intermediate endothermicities are also the processes with intermediate barriers. They correspond to substitution of H_2O trans to water (VII) or chlorine trans to Cl^- (III, I, VI). The corresponding Pt–CH_4 distances are also intermediate in length ranging from 2.94 Å (V) to 2.82 Å (III). The optimized structures for the five different methane complexes are shown in Fig. 5. We shall now turn to the dissociative substitution mechanism for methane uptake.
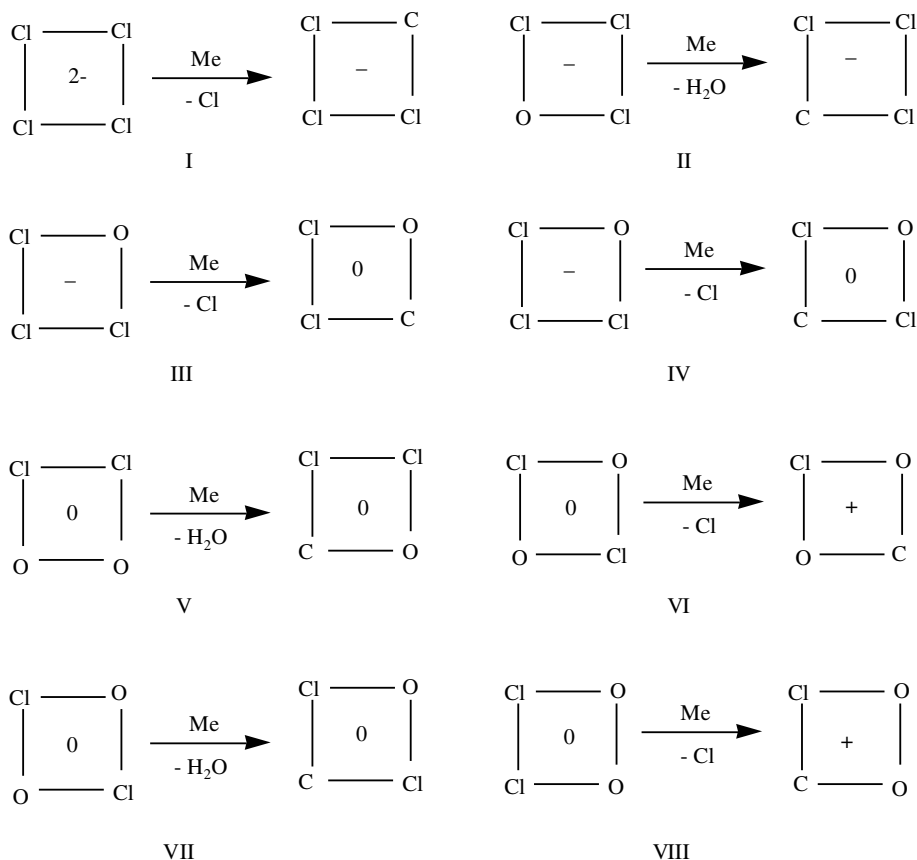
Scheme 5. Possible methane uptake reactions involving $PtCl_4^{2-}$, $PtCl_3(H_2O)^-$ and $PtCl_2(H_2O)_2$.

Table 2
Calculated thermodynamic and kinetic data for associative methane uptake[f]

Reactions[c]	Reactant[d]			Transition state[e]			Product[e]		
	ΔG	ΔH	$\Delta S^{a,b}$	$\Delta G^{\ddagger}$	$\Delta H^{\ddagger}$	$\Delta S^{\ddagger a,b}$	ΔG	ΔH	$\Delta S^{a,b}$
I	0	0	0	31.58	27.50	−14.12	11.81	14.87	9.81
II	2.81	5.06	7.09	23.26	18.64	−15.46	9.00	9.81	2.72
III	2.81	5.06	7.09	32.98	27.06	−19.83	16.70	19.09	8.03
IV	2.81	5.06	7.09	37.77	33.41	−14.59	19.98	22.59	8.78
V	7.95	11.62	11.84	24.96	20.76	−14.05	11.56	12.53	3.28
VI	7.72	11.20	11.22	33.39	28.43	−16.58	22.03	25.36	11.16
VII	7.72	11.20	11.22	30.68	26.08	−16.17	15.07	16.45	4.65
VIII	7.95	11.62	11.84	35.24	31.20	−13.55	22.97	25.87	9.75

[a] ΔG and ΔH in kcal/mol.
[b] ΔS in cal/mol K.
[c] For numbering of reactions, see Scheme 5.
[d] Relative to $PtCl_4^{2-}$.
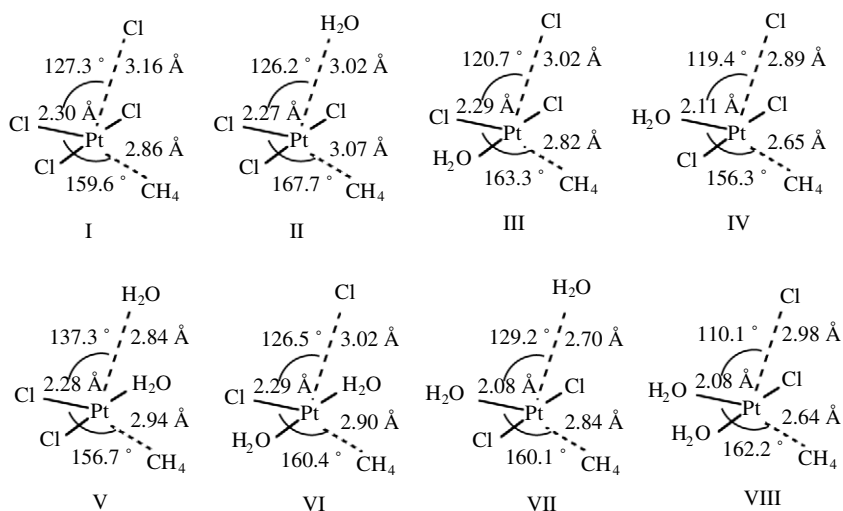[e] Relative to reactants.
[f] Calculated at 298 K.

Fig. 2. Geometry of the transition states for the eight associative pathways leading to methane uptake.

3.4. Dissociative mechanism for methane uptake

In the dissociative mechanism, the leaving group (H_2O or Cl^-) has completely departed before the uptake of methane (Scheme 3). We present in Table 3 the thermodynamic and kinetic data for the eight (I–VIII) methane uptake reactions (Scheme 5) along the dissociative path. The second column of Table 3 affords the free energy ($\Delta G_1^{\ddagger}$), enthalpy ($\Delta H_1^{\ddagger}$) and entropy ($\Delta S_1^{\ddagger}$) of activation for the dissociation of the first ligand (H_2O or Cl^-) whereas column 3 provides the corresponding free energy (ΔG_1), enthalpy (ΔH_1) and entropy (ΔS_1) of the reaction. Both ΔH_1 and ΔG_1 follow the same trend with II, V from the dissociation of H_2O trans to chlorine < I, III, VI from Cl^- dissociation trans to chlorine < VII from H_2O trans to H_2O < IV, VIII from Cl trans to H_2O. Exactly the same trends are observed for $\Delta H_1^{\ddagger}$ and $\Delta G_1^{\ddagger}$. These are also the trends for ΔH_1, ΔG_1 and $\Delta H_1^{\ddagger}$, $\Delta G_1^{\ddagger}$ in the case of the associative mechanism, see Table 2.

We note that the first dissociation reaction has a kinetic barrier as both $\Delta G_1^{\ddagger}$ and $\Delta H_1^{\ddagger}$ are larger than, respectively, ΔG_1 and ΔH_1. The enthalpic barrier $\Delta H_1^{\ddagger}-\Delta H_1$ comes form the fact that the leaving ligand L first obtains its full solvation energy after complete dissociation. The enthalpic barrier is somewhat smaller (7 kcal/mol) for the two facile reactions II, V than for the remaining sets (10 kcal/mol). The free energy barrier $\Delta G_1^{\ddagger}-\Delta G_1$ has further contributions from the translational and rotational entropy generated as the leaving group completely dissociate. The entropic factors, $\Delta G_1^{\ddagger}-\Delta G_1$, make 5–7 kcal/mol larger than $\Delta H_1^{\ddagger}-\Delta H_1$.

Also shown in Table 3 is the free energy ($\Delta G_2^{\ddagger}$), enthalpy ($\Delta H_2^{\ddagger}$) and entropy ($\Delta S_2^{\ddagger}$) of activation, for the (second) methane uptake transition state relative to the intermediate Pt(X)(Y)(L) of Scheme 3. We note that the internal enthalpic barrier for methane uptake $\Delta H_2^{\ddagger}$ is nearly constant (∼13–16 kcal/mol). It originates from the loss of solvation energy as methane is combined with the tri-coordinated

Table 3
Calculated thermodynamic and kinetic data for dissociative methane uptake[f]

Reactions[c]	Reactant[d]			Transition state 1[e,g]			Intermediate 1[e,h]			Transition state 2[i,j]		
	ΔG_0	ΔH_0	$\Delta S^{a,b}$	$\Delta G_1^\ddagger$	$\Delta H_1^\ddagger$	$\Delta S_1^{\ddagger a,b}$	ΔG_1	ΔH_1	$\Delta S_1^{a,b}$	$\Delta G_2^\ddagger$	$\Delta H_2^\ddagger$	$\Delta S_2^{\ddagger,a,b}$
I	0	0	0	23.53	23.89	0.76	4.92	13.29	27.60	19.17	14.28	−16.38
II	2.81	5.06	7.09	12.61	13.48	2.55	2.11	8.23	20.51	19.17	14.28	−16.38
III	2.81	5.06	7.09	20.01	19.78	−0.76	6.90	14.37	25.04	19.22	14.61	−15.43
IV	2.81	5.06	7.09	31.58	32.29	2.34	15.38	22.13	22.65	19.46	15.12	−14.56
V	7.95	11.62	11.84	12.37	13.34	2.78	1.76	7.81	20.29	17.56	14.61	−9.43
VI	7.72	11.20	11.22	24.51	24.38	−0.45	7.00	14.83	26.25	18.91	14.54	−14.63
VII	7.72	11.20	11.22	26.70	26.83	0.4	10.47	15.99	18.54	19.46	15.12	−14.58
VIII	7.95	11.62	11.84	29.82	29.71	−0.31	12.82	21.39	28.76	21.28	15.46	−19.10

[a] ΔG and ΔH in kcal/mol.
[b] ΔS in cal/mol K.
[c] For numbering of reactions see Scheme 5.
[d] Relative to $PtCl_4^{2-}$.
[e] Relative to reactants.
[f] Calculated at 298 K.
[g] Transition state for dissociation of leaving ligand L, see Scheme 3.
[h] Three coordinated Pt(X)(Y)(T), see Scheme 3.
[i] Transition state for uptake of CH_4 by intermediate Pt(X)(Y)(T), see Scheme 3.
[j] Relative to intermediate Pt(X)(Y)(T).
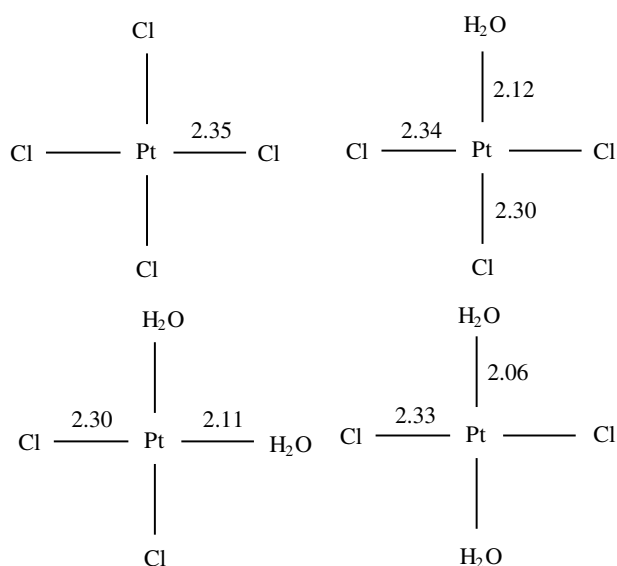
Fig. 3. Optimized structures of $PtCl_4^{2-}$, $PtCl_3(H_2O)^-$ and $PtCl_2(H_2O)_2$.

platinum species. The internal free energy barrier $\Delta G_2^\ddagger$ has in addition an entropic contribution (3–5 kcal/mol) due to the loss of translational and rotational entropy. The structures for the five unique transition states for methane uptake are shown in Fig. 4. Because Cl^- is a stronger *trans*-directing ligand than H_2O, the Pt–CH_4 distance is longer (2.70 Å) when CH_4 is *trans* to Cl than when CH_4 is *trans* to H_2O (2.60 Å).

3.5. Comparison of dissociative and associative methane uptake

Up to now, we have not compared the relative rate of associative and dissociative methane uptake. To this end, we note that the rate expression for dissociative methane uptake in Eq. (4) can be simplified when we observe that the barrier $\Delta G_1^\ddagger - \Delta G_1$ for the recapture of the leaving group L by the intermediate PtXYT is smaller than the barrier $\Delta G_2^\ddagger$ for the capture of CH_4 by PtXYT. We can thus assume in Eq. (4) that $k_{-1} > k_2$. In this case, k_D of Eq. (4) reduces to

$$k_D \sim \frac{k_1 k_2}{k_{-1}} \frac{[CH_4][PtXYTL]}{[L]} = K_1 k_2 \frac{[CH_4[PtXYTL]}{[L]}, \quad (7)$$

where K_1 is the equilibrium constant for dissociation of L from PtXYTL.

Putting aside for the moment the factor 1/[L] by setting [L] = 1, we can compare the rate constant k_A for the associative mechanism with the effective rate constant k_D for the dissociative mechanism of Eq. (7).

Alternatively, we can compare the activation parameters $\Delta G_D^\ddagger = \Delta G_1 + \Delta G_2^\ddagger$; $\Delta H_D^\ddagger = \Delta H_1 + \Delta H_2^\ddagger$; $\Delta S_D^\ddagger = \Delta S_1 + \Delta S_2^\ddagger$ given in Table 3 for dissociative CH_4 uptake with the corresponding parameters $\Delta G^\ddagger$, $\Delta H^\ddagger$ and $\Delta S^\ddagger$ of Table 2 for the associative CH_4 uptake.

We find not surprising that $\Delta S_D^\ddagger$ is positive where $\Delta S_A^\ddagger$ is negative. Also the free energy of activation for the different processes follows the same order for the two mechanisms. Thus, the most facile CH_4 uptake processes correspond to the replacement of H_2O *trans* to Cl^- in II and IV of Scheme 5 by CH_4. All the other substitution processes have higher barriers. For II and IV, the dissociative mechanism seems more favorable with a free energy of activation that is lower by 3 kcal/mol. This conclusion is not likely to change when the factor 1/[L] is taken into account with L = H_2O. However, the inherent error sources of our calculations, especially with regard to estimating contributions from entropy and solvation, do not allow us firmly to favor the dissociative mechanism. The many substitution reactions involving the displacement of Cl^- are less favorable and not likely to play a role in the Shilov
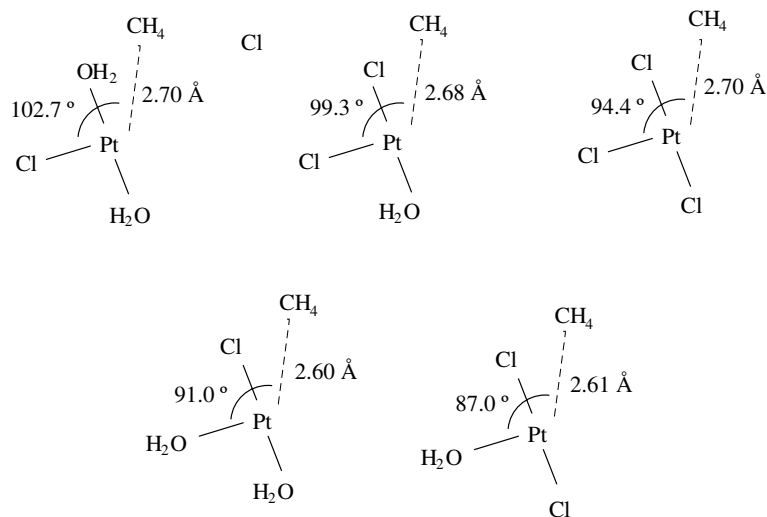
Fig. 4. Geometry of the transition states for methane uptake in the dissociative mechanism.
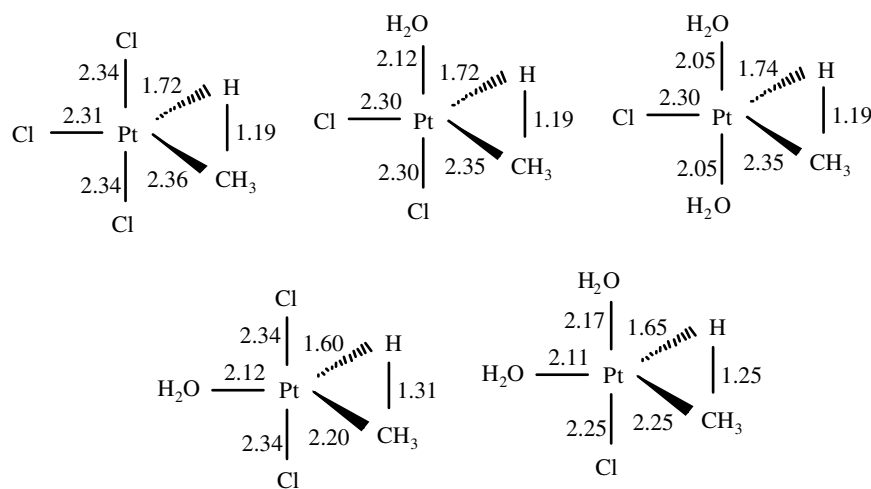

Fig. 5. Optimized structures for the five different methane complexes.

chemistry. For these processes, dissociation seems again favorable, especially if we take into account the 1/[L] factor for L = Cl⁻.

3.6. C–H activation

The uptake of CH_4 to the platinum center results in a methane platinum complex that serves as a precursor for C–H activation with a C–H bond coordinated in a η^2-conformation to the metal. It follows from our previous discussion (Fig. 5) that as much as five different methane complexes can form under the conditions given by Shilov and co-workers [1] and Gol'dshleger and Shteinman [7], respectively. Here, three have chlorine *trans* to CH_4 whereas the *trans* position for the two remaining species is taken up by H_2O. The five different C–H activation processes corresponding to the possible methane complexes are shown in Scheme 6 and the related kinetic and thermodynamic data are displayed in Table 4.

All the C–H addition reactions are exothermic, see Table 4. Those with the C–H bond adding *trans* to chlorine have enthalpies of −6 kcal/mol to −8 kcal/mol whereas the addition of a C–H bond *trans* to H_2O gives rise to reaction enthalpy of −13 kcal/mol. The addition of a C–H bond *trans* to H_2O is more favorable as H_2O is less *trans* destabilizing than chlorine and thus weakens the Pt–CH_3 bond to a lesser extend than chlorine. It is consistent with this observation that the Pt–CH_3 bond in the final hydrido methyl complex is shortest with H_2O in the *trans* position, see Fig. 6.

The three C–H activation processes in which methane adds *trans* to chlorine all have early transition states as one would expect for exothermic processes. It is further interesting to observe that the most exothermic processes (2 of Scheme 6) has the smallest barrier and the least exothermic process (3 of Scheme 6) the highest barrier, as one would expected for a sense of related exothermic reactions. Based on the above discussion of the barriers for C–H activation *trans* to chlorine, one would expect that the most
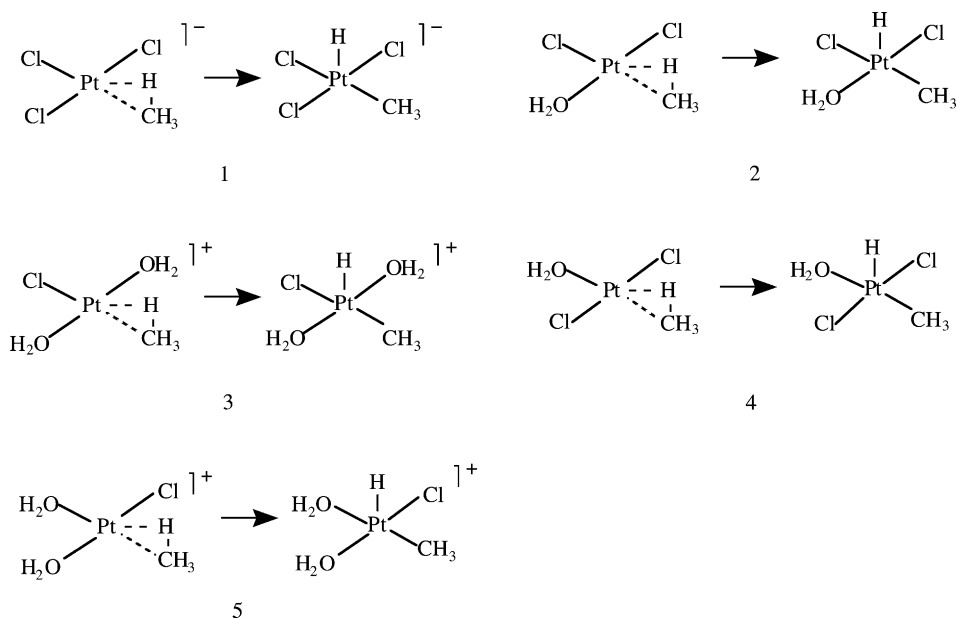
Scheme 6. Possible C–H activation steps in the Shilov and Shteinman reactions.

Table 4
Calculated thermodynamic and kinetic data for C–H activation[f]

Reactions[c]	Reactant[d]			Transition state[e]			Product[e]		
	ΔG	ΔH	$\Delta S^{a,b}$	ΔG_1	ΔH_1	$\Delta S_1^{a,b}$	ΔG	ΔH	$\Delta S^{a,b}$
1	11.81	14.87	9.81	1.10	2.50	4.72	−6.96	−7.03	−0.23
2	16.70	19.09	8.03	0.75	2.11	4.57	−7.81	−7.99	−0.60
3	22.03	25.36	11.16	4.96	4.06	−2.99	−6.44	−6.95	−1.70
4	15.07	16.45	4.65	–	–	–	−13.61	−13.95	−1.14
5	22.97	25.87	9.75	–	–	–	−13.82	−14.20	−1.27

[a] ΔG and ΔH in kcal/mol.
[b] ΔS in cal/mol K.
[c] For numbering of reactions, see Scheme 6.
[d] Data from Table 2.
[e] Relative to reactants.
[f] Calculated at 298 K.

exothermic addition of CH_4 *trans* to H_2O should have an even lower barrier. In fact we find the barrier is so low that we are unable to detect it with the computational methods used here, see Table 4.

A more detailed comparison between the structures of the methane complexes (Fig. 5) and the transition state structures for C–H activation (Fig. 6) reveals that when chlorine is *trans* to CH_4, the Pt–C bond length is about 2.35 Å in the methane complex and it decreases by about 0.25 Å in going to the transition state. However, with H_2O *trans* to CH_4, C is 0.15 Å closer to the platinum because of the weaker *trans*-directing effect of H_2O and we can anticipate that Pt–C bond length decreases by a lesser extend to reach the transition state. So, with H_2O as the *trans* ligand to methane, C–H activation of methane should have a lower barrier compared with Cl, a stronger *trans*-directing ligand, *trans* to methane (see Fig. 7).

Fig. 8 displays a simplified correlation diagram for the C–H activation process discussed above. We illustrate for

simplicity the lobes of the σ and σ^* orbitals of the activated C–H bond by the σ and σ^* orbitals of H_2. Also, only the orbitals that experience a change in occupation during the reaction are shown. They are at the start of the reaction, the empty σ^* orbital of the σ-bond that is about to be broken and the occupied $d_{x^2-y^2}$ metal orbital (a_1) that is about to loose two electrons during the oxidative addition process. The occupied $d_{x^2-y^2}$ orbital correlates with the empty anti-bonding d_{z^2} orbital on the product side and the degree of antibonding character is directly proportional to the labilizing ability of the *trans*-directing ligand T. As the process proceeds the energy will rise, as the occupied $d_{x^2-y^2}$ orbital correlates to the anti-bonding d_{z^2} orbital. The rise will be proportional to the labilizing ability of T. Eventually b_1 will cross a_1 in energy and the two electrons can jump to b_1 that becomes a non-bonding ligand orbital.

It follows from our calculations that the transition state energy for C–H activation is much lower than that for
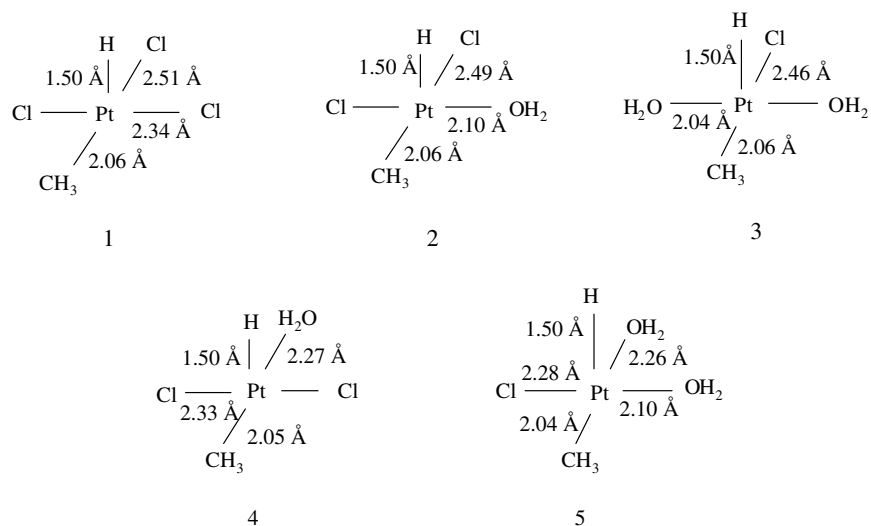
Fig. 6. Structures of the methyl hydrido platinum complexes after C–H activation.
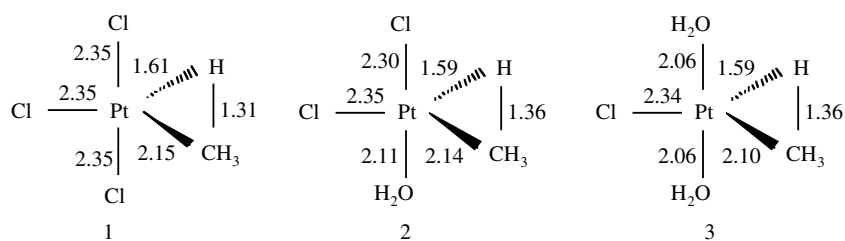

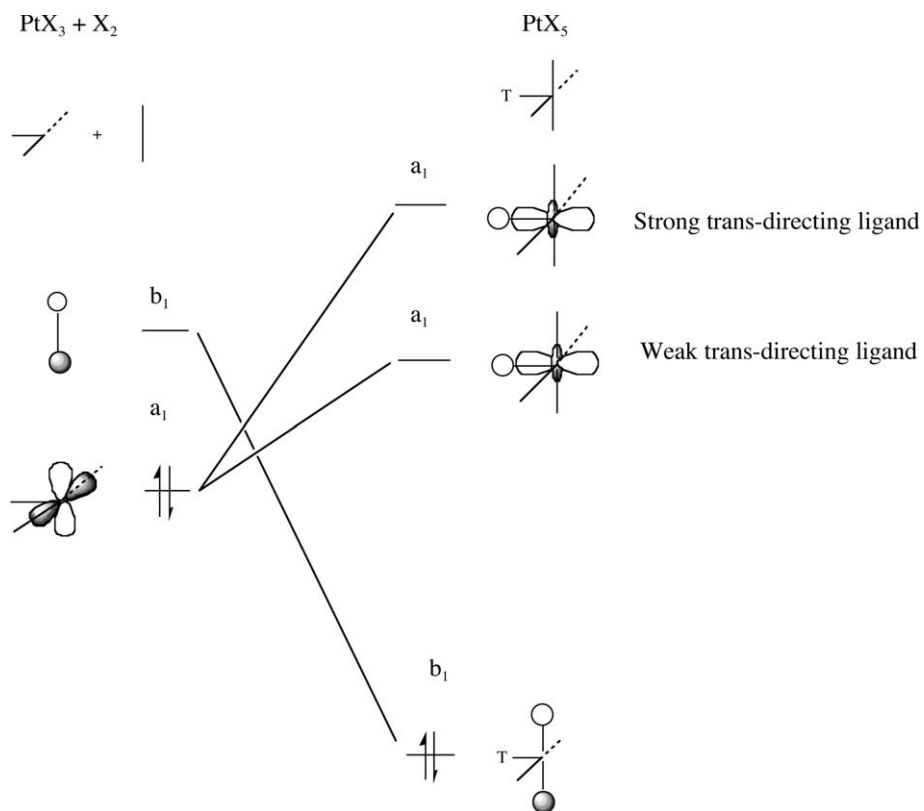Fig. 7. Transition states for the C–H activation.

Fig. 8. Correlation diagram of C–H activation of tri-coordinated platinum and methane.

either associative or dissociative uptake of CH_4. We must thus conclude that uptake rather than C–H activation is rate determining under Shilov reaction conditions.

3.7. Overall rate of the Shilov reaction

It follows from the previous discussion that the three dominating species under Shilov conditions are $PtCl_4^{2-}$ (95.8%), $PtCl_3(H_2O)^-$ (4.1%) and $PtCl_2(H_2O)_2$ (5×10^{-3}%). Thus, the overall rate for H^+/D^+ exchange is

$$k_{eff} = [\% \ \alpha]k_\alpha + [\% \ \beta]k_\beta + [\% \ \delta]k_\delta,$$

where we refer to the three species $PtCl_4^{2-}$, $PtCl_3(H_2O)^-$ and $PtCl_2(H_2O)_2$ as α, β and δ, respectively, and k_α, k_β and k_δ refer to the rate constants for the rate-determining CH_4 uptake process involving the three species in the H^+/D^+ exchange reaction.

For $PtCl_3(H_2O)^-$, there are three different uptake pathways. However, II of Scheme 5 where H_2O is replaced by CH_4 has the lowest barrier and will thus predominate. For $PtCl_2(H_2O)_2$, V of Scheme 5 where again H_2O is replaced by CH_4 will be the prevailing uptake pathway.

For the dissociative mechanism, reaction rate of each platinum species is proportional to its concentration in the solution. Although $PtCl_2(H_2O)_2$ has the lowest reaction barrier, its extremely low concentration (~0.005%) dramatically reduces its rate. The rate ratio for $PtCl_4^{2-}$, $PtCl_3(H_2O)^-$ and $PtCl_2(H_2O)_2$ is 150:60:1. $PtCl_4^{2-}$ is the most active species. The highest concentration of $PtCl_4^{2-}$ (95.8%) makes it the main contribution (98%) to the overall rate. The overall rate of the dissociative mechanism is $k_D = 16.16 \ h^{-1}$.

For the associative mechanism, $PtCl_3(H_2O)^-$ and $PtCl_2(H_2O)_2$ have similar energy barriers, but higher concentration of $PtCl_3(H_2O)^-$ makes it the most active species. The rate ratio for $PtCl_4^{2-}$, $PtCl_3(H_2O)^-$ and $PtCl_2(H_2O)_2$ is $1:10^4:1$. The low rate k_α of $PtCl_4^{2-}$ now makes its contribution to k_{eff} negligible. Thus, $PtCl_3(H_2O)^-$ is the main contributor in the associative reaction (~99.99%). The overall rate for the associative mechanism is $k_A = 0.02 \ h^{-1}$, which compares favorably to the experimental value of $0.3–0.4 \ h^{-1}$ at 100 °C.

Under Gol'dshleger and Shteinman [7] conditions, where $PtCl_2(H_2O)_2$ is added to an acidic aqueous solution, $PtCl_2(H_2O)_2$ is the most active species because of its high concentration and lowest reaction barrier. So, $PtCl_2(H_2O)_2$ contributes the most to the overall rate, no matter in dissociative or associative mechanism. The overall rate for the dissociative mechanism is $k_D = 3.28 \ s^{-1} \ mol^{-1}$ correspond to $k_A = 1.64 \times 10^{-3} \ s^{-1} \ mol^{-1}$ for the associative mechanism. In Shteinman's work, $PtCl_2(H_2O)_2$ was also found to be the most active species and the rate of H/D exchange of cyclohexane was given as $7.42 \times 10^{-3} \ s^{-1} \ mol^{-1}$. The comparison of the rates of cyclohexane and methane shows that cyclohexane reacts about 10 times faster than methane does.

Gol'dshleger and Shteinman [7] find for $PtCl_2(H_2O)_2$ that the enthalpy and entropy of activation for the H/D exchange are 17 kcal/mol and -22.6 cal/mol K, respectively. These values are in good agreement with our theoretical estimates of 20.8 kcal/mol and -14.1 cal/mol K for the associative uptake of CH_4 by $PtCl_2(H_2O)_2$.

All the above data show that associative mechanism matches better with the experimental results. Associative mechanism is a one step process, energy barrier only depends on the transition state. For the two-step dissociative mechanism, energy barrier depends not only on the transition state at the second step which is methane uptake, but also on the energy of the intermediate ions formed in the first step after one ligand is completely dissociated. The inherent error sources of our calculations, especially with regard to estimating contributions from entropy and solvation, will affect more to the dissociative mechanism and make its energy barrier lower. Although dissociative mechanism has lower barrier, but associative mechanism should be more likely due to its good match with the experimental results and lower influence by the inherent source of error in the calculation.

4. Concluding remarks

The Shilov reaction in which $PtCl_4^{2-}$ will catalyze H/D exchange of alkanes in acidic aqueous solution has been investigated using DFT (density functional theory). We have found that $PtCl_4^{2-}$, $PtCl_3(H_2O)^-$ and $PtCl_2(H_2O)_2$ are the three main species present after $PtCl_4^{2-}$ is added to water. Methane uptake has been found to be the rate-determining step in the Shilov reaction. Both a dissociative and an associative mechanism were considered for the methane uptake. Although calculated results slightly favor the dissociative pathway, we were not able to exclude a possible associative mechanism due to uncertainties in the calculated contributions to the free energies of activation from entropy and solvation. The overall rate of the Shilov reaction has also been determined for both the dissociative and associative mechanisms. The most species in the reaction depends on both the reaction barrier of the H/D exchange reaction and its concentration in the solution. For the dissociative pathway, $PtCl_4^{2-}$ contributes the most to the overall rate, on the other hand, $PtCl_3(H_2O)^-$ with the higher rate contributes more than $PtCl_4^{2-}$ for the overall rate of the associative pathway. The extremely low concentration of $PtCl_2(H_2O)_2$ makes its contribution in overall rate negligible in both cases. The experimental and theoretical rates agree well for the associative mechanism.

Under Shteinman reaction conditions where $PtCl_2(H_2O)_2$ is added to an acidic aqueous solution, Methane uptake is still the rate-determining step and $PtCl_2(H_2O)_2$ is the most active species due to its dominant concentration. The overall rates for both the associative and dissociative mechanisms have been determined. Associative mechanism once again shows the best match with the experimental results.

Acknowledgements

References

[1] N.F. Gol'dshleger, M.B. Tyabin, A.E. Shilov, A.A. Shteinman, Zh. Fiz. Khim. (Engl. Transl.) 43 (1969) 1222.
[2] R.J. Hodges, D.E. Webster, P.B. Wells, J. Chem. Soc. A (1971) 3230.
[3] N.F. Gol'dshleger, V.V. Es'kova, A.E. Shilov, A.A. Shteinman, Zh. Fiz. Khim. (Engl. Transl.) 46 (1972) 785.
[4] P.E.M. Siegbahn, R.H. Crabtree, J. Am. Chem. Soc. 118 (1996) 4442.
[5] K. Mylvaganam, G.B. Bacskay, N.S. Hush, J. Am. Chem. Soc. 122 (2000) 2941.
[6] L. Johansson, M. Tilset, J.A. Labinger, J.E. Bercaw, J. Am. Chem. Soc. 122 (2000) 10846.
[7] N.F. Gol'dshleger, A.A. Shteinman, React. Kinet. Catal. Lett. 6 (1977) 43.
[8] A. Becke, Phys. Rev. A 38 (1988) 3098.
[9] J.P. Perdew, Phys. Rev. B 34 (1986) 7406.
[10] J.P. Perdew, Phys. Rev. B 33 (1986) 8822.
[11] G. Te Velde, F.M. Bickelhaupt, E.J. Baerends, S. van Gisbergen, C.F. Guerra, J.G. Snijders, T.J. Ziegler, Comput. Chem. 22 (2001) 931.
[12] T. Ziegler, V. Tschinke, E.J. Baerends, J.G. Snijders, W. Ravenek, J. Phys. Chem. 93 (1989) 3050.
[13] D.A. McQuarrie, Statistical Thermodynamics, Harper, New York, 1973.
[14] W.R. Fawcett, J. Phys. Chem. B 103 (1999) 11181.
[15] A. Klamt, G. Schuurmann, J. Chem. Soc., Perkin. Trans. 2 (1993) 799.
[16] C.C. Pye, T. Ziegler, Theor. Chem. Acc. 101 (1999) 396.
[17] W.E. Dasent, Inorganic Energetics, Penguin, Middlesex, UK, 1970.
[18] D.H. Wertz, J. Am. Chem. Soc. 102 (1980) 5316.
[19] D.R. Lide (Ed.), CRC Handbook of Chemistry and Physics, 76th ed., CRC Press, New York, 1995.
[20] L.I. Elding, I. Leden, Acta Chem. Scand. 20 (1966) 706.
[21] L. Drougge, L.I. Elding, L. Gustafson, Acta Chem. Scand. 21 (1967) 1647.
[22] L.I. Elding, Acta Chem. Scand. 24 (1970) 1331.
[23] C.I. Sanders, D.S. Martin, J. Am. Chem. Soc. 83 (1961) 807.
[24] J. Procelewska, A. Zahl, R.V. Eldik, H.A. Zhong, J.A. Labinger, J.E. Bercaw, Inorg. Chem. 41 (2002) 2808.
[25] J.S. Coe, MTP Int. Rev. Sci.: Inorg. Chem. 2 (1974) 45.
[26] L.I. Elding, Inorg. Chim. Acta 7 (1973) 581.
[27] R.J. Cross, Chem. Soc. Rev. 14 (1985) 197.